

40 Key words: Upper Rhine Graben, Riedseltz-Landau normal fault, cataclasite, fractured grains.

41

42 The Upper Rhine Graben (URG) and Lower Rhine Embayment (LRE) are major
43 intraplate seismically active tectonic zones in the European plate interior with low
44 deformation rates ≤ 1 mm/yr (Stein et al., 2015). Late Pleistocene and Holocene normal
45 faulting correlated with past earthquake activity and surface ruptures have revealed the
46 potential for $M_w \geq 6.5$ earthquakes (Camelbeeck and Meghraoui, 1998; Meghraoui et al.,
47 2001; Vanneste et al., 2001; Ferry et al., 2005; Grützner et al., 2016). Identified fault scarps
48 with cumulative surface slip in the URG and LRE correspond to crustal-scale normal fault
49 structures visible by means of recent seismicity distribution (Bonjer et al., 1984; Camelbeeck
50 and Van Eck, 1994) and seismic reflection data (Brun et al., 1992). In the URG, the active
51 deformation with strain distribution $\leq 10^{-10}$ and fault slip rate ≤ 0.5 mm/yr can be correlated
52 with a low-level of seismicity (Fig. 1; Ferry et al., 2005; Masson et al., 2010; Fuhrmann et al.,
53 2013). However, major fault segments delineating the graben edges that may generate large
54 intraplate earthquakes are poorly known.

55 Cataclasis is commonly believed to take place only along faults below depths of 500-
56 1000m (Fulljames et al., 1997; Bense et al., 2003, Petrik et al., 2014). However, recent studies
57 have shown that it is possible to develop cataclasis along faults in shallowly buried
58 unconsolidated sands (Heynekamp et al., 1999; Sigda et al., 1999; Cashman and Cashman
59 2000; Rawling et al., 2001; Rawling and Goodwin, 2003; 2006; Bense et al., 2003; Cashman
60 et al. 2007; Evans and Bradbury 2007; Sallet and Wibberley 2010) and tuffs (Wilson et al.,
61 2003; 2006). Cashman and Cashman (2000) and Cashman et al. (2007) have suggested that
62 the presence of cataclasis in unconsolidated sand can be used as an indicator of seismic slip.
63 Cashman et al. (2007) showed that at a location where the San Andreas fault is creeping, fault
64 zones cutting unconsolidated sand deform by grain rolling, whereas cataclastic deformation
65 bands are found along segments of the San Andreas fault that have deformed by stick slip in
66 large earthquakes. While deformation bands are not exclusively related to coseismic slip
67 (Balsamo and Storti 2011) the presence of cataclasis in very shallowly buried sediments that
68 have never experienced high confining stress may be an indicator of high dynamic stresses
69 during coseismic slip.

70 In this study we present evidence for young surface offsets and cataclasis within a
71 fault zone affecting unconsolidated late Pleistocene (loess) and Holocene deposits along the
72 western flank of the northern URG. The Riedseltz-Landau fault zone is exposed in an open pit
73 sand quarry situated about 1.5 km northeast of the town of Riedseltz village, and mapped

74 using fault scarp morphology crossing late Quaternary alluvial fans. Samples collected from
75 the fault zone in the quarry are analysed for microstructures and mineralogy highlighting the
76 evolution of the cataclastic deformation bands, slip surfaces and fractures. The potential link
77 between coseismic deformation and cataclasis in very shallowly buried unconsolidated sand
78 provides further evidence that this fault has hosted seismic events.
79

80 **Seismotectonic setting**

81 The NNE-SSW trending Upper Rhine graben (URG) is a section of the European
82 Cenozoic rift system developed in the foreland of the Alps (Fig. 1) and is approximately 300-
83 km long and up to 40 km wide (Illies, 1981). Subsidence and synrift sedimentation initiated in
84 the Eocene due to extension followed by sinistral transtension. Rifting is asymmetric with
85 larger fault displacements, and therefore deeper graben fill, on the eastern side of the northern
86 URG. The thickness of the Quaternary terrestrial clastic sediment sequences is variable with a
87 maximum (200 m) to the Northeast of our study area (Doebel, 1970). The northern URG
88 shows faults with clear geomorphological expression, bounding the footwall blocks of the
89 Black Forest to the east and the Vosges Mountains and Pfalzer Wald to the west (Illies, 1981).

90 The seismicity of the northern URG region is characterized by low to moderate
91 intraplate seismicity, although damaging earthquakes have occurred in the past (Fig. 1,
92 Bonjer, 1984; Leydecker, 2009; <http://www.sisfrance.net>). Instrumental and historical
93 earthquakes in the northern URG have apparently not been large enough to cause surface
94 rupture. However the seismogenic layer reaches 20-km-depth and observed fault segment
95 lengths sometimes exceed 20 km (Kervyn et al., 2002), implying a maximum moment
96 magnitude $M_w > 6.5$ (Leonard, 2010). With regards to the southern URG where the 1356
97 Basel earthquake ($M_w 6.5$) can be correlated to a paleoseismic rupture (Meghraoui et al.,
98 2001), the identification of active and seismogenic faults in the northern URG is problematic
99 due to the absence of known large historical earthquakes with surface ruptures. The
100 identification of fault scarps in the area is an issue due to the low slip rates (< 0.5 mm/yr.),
101 dense vegetation cover on mountains and hills, and the high impact of human activity (urban
102 areas and agricultural ploughing) on the geomorphology in valleys. Mapping of faults in the
103 basin has largely been due to seismic reflection and hydrocarbon exploration profiles (e.g.,
104 Illies, 1981; Brun et al., 1992; Behrmann et al., 2003). Some studies have focused explicitly
105 on Neogene and Quaternary fault movement with thinning of Quaternary units on the west
106 URG (Haimberger et al., 2005; Peters et al., 2005), though the likelihood of late Pleistocene

107 and Holocene earthquake activity in the region has increasingly being investigated (Lemeille
108 et al., 1999; Kervyn et al., 2002; Ferry et al., 2005; Nivière et al., 2008; Baize et al., 2013).

109
110

111 **The Riedseltz-Landau fault zone**

112 The Riedseltz-Landau fault zone is a north-south trending steep and composite scarp
113 bounding the western flank of the northern URG (Fig. 2a). The fault was not previously
114 identified as an active and seismogenic structure. Seismic profiles (Fig. 2b and c) display
115 normal fault geometry that offset (> 500 m) Oligocene-Miocene units at $\sim 1.5 - 2.0$ -km-depth.
116 However at the surface the fault appears as a subtle geomorphic lineament structure that
117 separates a higher plateau of basement Hercynian rocks (Vosges Mountains) on the west from
118 lower levels of alluvial fans and fluvial Rhine units to the east. Triangular facets bounding the
119 Vosges Mountain front and cumulative scarps affecting late Quaternary alluvial fans can be
120 traced into the basin along fault scarps. In his neotectonic analysis conducted along the west
121 URG mountain front, Monninger (1985) describes faults in three quarries at Klingenmünster,
122 Barbelroth and Riedseltz affecting upper Pleistocene units with 1.5 to 3.25 m vertical offset.
123 South of Wissembourg, the fault is exposed in the Riedseltz quarry (Lat. 49.00, Long. 7.96),
124 and can be traced for 12-15 km to the south (Fig. 2a and 2c). North of Wissembourg, the fault
125 has two branches with 1) a main strand following the mountain front and extending northward
126 within the basement rocks of the Vosges Mountains until the Leistadt region where it joins the
127 Worms fault scarps (Fig. 2a), and 2) a subtle cumulative scarp located about 3 to 5 km east of
128 the previous fault trace reaching ~ 20 -m-high and affecting late Quaternary alluvial fans
129 immediately west of Landau. North of Landau city and along the mountain front at Forst,
130 Weidenfeller and Zöller (1995) show faulted alluvial deposits and paleosol units with
131 Thermo-luminescence dating spanning from 88 ka to 284 ka. Further north along the west
132 URG border, the fault zone extends for ~ 70 km and displays two distinct topographic scarps
133 across Wachenheim and Worms regions. Field investigations on the west URG escarpment
134 with tectonic geomorphology (Kervyn et al., 2002) and trenching with radiocarbon dating
135 (Peters, 2007) provide evidence of fault activity between 8 ka and 14 ka. The late Pleistocene
136 and Holocene fault activity is also attested by subsidence observed by Illies and Greiner
137 (1979) and Monninger (1985) who suggest a possible correlation with the 8 October 1952
138 earthquake (Io VIII MKS; estimated $M_w < 5.5$; see Fig. 1).

139

140 **The Riedseltz fault zone exposure**

141 The fault escarpment that cuts late Pleistocene and Holocene units at the surface is
142 exposed at the Riedseltz quarry. Pliocene sandy gravel, is overlain by ~20-m-thick loess
143 (sandy) units, which in turn are overlain by ~10-m-thick sandy-clay deposits. According to
144 BRGM (1977), the loess units belong to the middle and late Quaternary (Riss and Würm
145 glacial classification, respectively), and the alluvial and colluvial sandy-clay units are
146 Holocene (Fig. 2d). The fault zone exposed in quarry is also visible in shallow (0 to 5-m-
147 depth) geophysical data (Ground Penetrating Radar, seismic reflection, seismic refraction and
148 electrical resistivity profiles from Bano et al., 2002). Bano et al. (2002) report that the fault
149 cuts the boundary between Pliocene sands and the overlying loess-alluvial units with a total
150 vertical offset of ~1.5 m along a fault oriented 165/60E. The quarried face trends
151 approximately east-west, exposing an east-dipping fault zone in cross section (Fig. 3a). The
152 bedding in the lower sand unit is obviously cut off against the fault and bedding dip steepens
153 into the fault zone. Due to the quarry activity, the footwall of the fault is almost entirely
154 covered with quarrying debris so sedimentary units could not be correlated across the fault.
155 Bano et al. (2002) used the shallow geophysical profiles to trace the fault for 50 m to the north
156 and 750 m to the south of the exposed cross section and showed that in the southern half of
157 the quarry the fault splits into two strands both of which offset the Loess and overlying
158 alluvial stratigraphy.

159 Consistent with observations of Monninger (1985), the fault is comprised of a central
160 zone of relatively structureless, mottled, mixed sand bounded on either side by localised fine-
161 grained, clay-rich and iron stained slip-surfaces (Fig. 3b). The width of this mixed zone is
162 variable, narrowing from 70 cm at the top of the exposure to 20 cm at the base over a distance
163 of 2 metres. The slip-surfaces are covered in a veneer of clay up to 5 mm thick that is
164 sometimes rather patchy. The main fault zone also contains closely spaced deformation bands
165 (Fig. 4a and b). In the hangingwall, pale deformation bands that offset bedding by up to 1 cm
166 are distributed around the fault core to a distance of 1.10-1.15 m. These deformation bands
167 have rather irregular traces when compared to bands formed in well-cemented sandstones
168 (e.g. Fossen et al. 2007). The sand within the fault zone is variably stained bright yellow,
169 orange and brown. The boundaries between different alteration colours are very sharp where
170 clay-rich slip surfaces occur, but are more diffuse elsewhere. Deformation bands also act as
171 abrupt boundaries for the colour variations in the host sandstone. Dark brown and black Fe-
172 oxide concretions are particularly concentrated along the slip surfaces.

173 Measurements of excavated slip surfaces show steep dip to the east with a mean of
174 181/72E (inset, Fig 3) consistent with the geophysical observations of Bano et al. (2002).

175 When the outcrop is carefully excavated to show a view onto the slip-surface face it can be
176 seen that the oxide mineralisation appears to have been streaked out, which may be a proxy
177 for slickenlines (Fig 4b). Due to the looseness of the deposits it was not possible to take
178 accurate slip vector measurements but the streaks are oriented in the down dip direction,
179 consistent with normal faulting.

180

181

182 **Deformation bands and microfractures in the fault zone**

183 Determining if these faults have cataclastic microstructures similar to those that
184 Cashman et al. (2007) link to seismic activity requires a detailed study of the host sediments
185 and the deformed fault rocks. Specimens of the undeformed host sediment (late Pleistocene
186 loess) were sampled using hand-tools to scoop out the almost completely unconsolidated
187 sand. Lumps of the more consolidated, and therefore more easily sampled, fault sand were
188 broken off with hand tools and tightly wrapped in duct tape to preserve the sample integrity
189 for thin sectioning. Samples were impregnated with resin in a vacuum chamber before curing.
190 The morphology of the deformed sand was observed in thin section using an optical
191 microscope and SEM, and by 3D grain analysis on the SEM. Friable samples are dried in the
192 oven at 60°C for 2-3 hours. They are then coated with Buehler EpoHeat epoxy resin and
193 returned to the oven for 2-3 hours for the resin to cure. The sample is sliced to approximately
194 1cm, and again dried for 1-2 hours before being treated again with resin and set again before
195 preparing the thin section.

196 The host sediments are fine to medium grained, moderately well sorted and sub-
197 rounded sands. They are cross-bedded with occasional metre thick coarse-grained incised
198 channels. The sand consists of 70% single crystal or polycrystalline quartz grains, with 20%
199 lithic grains and 10% feldspar (from CL analysis). Strained quartz grains are common with
200 undulose extinction and mylonitic fabrics, consistent with a metamorphic source for much of
201 the sediment. The host sand grains range from sub-angular to rounded. Quartz overgrowths
202 are occasionally seen but their irregular distribution and the high clay content of the matrix
203 suggests that these may have been reworked from older, more cemented sand into these
204 sediments. Occasional oxide-cemented lithic grains are also likely to have been reworked.
205 Throughout the quarry the sands have been stained a variety of shades of pale yellow to
206 orange (Fig. 3b). The colour banding can be seen to cross cut the bedding in the host sands
207 (e.g. Fig. 3b – bottom left hand corner) so the staining is therefore post-depositional. From
208 sieving and thin-section analysis the maximum grain size in both the host sand and the

209 deformed sand is ~ 1 mm. The modal grain size of the host sands determined by sieving range
210 from 0.25mm to 0.125mm.

211 The deformation bands are localised zones of significant grain size reduction a few
212 mm wide that contain highly angular grains (Fig. 5a, b and c). These zones still contain
213 rounded grains but these are mostly over 0.25mm in diameter and the smaller grains
214 (<0.25mm) show significantly more angularity than in the host rock. The preservation of
215 'survivor grains' surrounded by more angular fragments is a common feature of cataclastic
216 deformation bands. Many of the quartz grains have fresh conchoidal fractures at the edge of
217 the grain. These appear as elongate flakes of quartz, with some partially attached to the grain
218 (Fig. 6). This is similar to the grain spalling reported by Rawling and Goodwin (2003), which
219 is diagnostic of grain fracturing under low confining pressures. Some transgranular fractures
220 are also preserved. The deformation band zones clearly have reduced porosity with respect to
221 the host rock (Fig. 5c). The striking colouration of the deformation zone observed in Figures
222 3, 5 and 7 is due to a strongly coloured matrix in the fault zone rocks. Matrix colour ranges
223 from bright orange to black and each matrix type has a consistent proportion of fine grains
224 (<0.05mm). The orange matrix contains streaks of yellow and brown colours in plain
225 polarized light (Fig. 7a), while in cross-polarized light it has medium to high birefringence
226 colours. A major character of the orange matrix is its 'flowing' appearance (Fig. 7b) and it
227 often mixes with a less obvious matrix that mostly consists of fine grains. The black matrix is
228 opaque and contains few to no fine grains. In thin section the black matrix often appears
229 fractured with some of these fractures being filled by the orange matrix (Fig. 7c). Within the
230 black matrix the grains are dominantly sub- angular to angular and are mostly >0.25mm with
231 very little finer grains (<0.05mm) and a notable lack of grain contacts (Fig. 7d). The grains
232 here, regardless of size, appear to be largely sub-angular to angular throughout, with only a
233 few grains appearing to be rounded. In these matrix-supported zones have up to 40% black
234 matrix.

235 Geochemical element spot analysis on the SEM shows that the orange matrix is
236 dominated by clays while the black matrix is predominantly Fe-rich oxide (Fig 8). XRD
237 analyses of three sets of powdered samples (hangingwall, footwall and fault zone) show that,
238 in agreement with the microstructural observations, quartz dominates the XRD diffraction
239 patterns to the extent that other minerals cannot be identified. Results for the clay size fraction
240 (<2µm) show little variation in clay composition between the samples within the fault and
241 those outside the fault (Fig. 9). The dominant peaks are 12.3 and 24.9 2θ, which indicates
242 kaolinite, although Fe-chlorite cannot be ruled out as these are difficult to distinguish in

243 mixtures using XRD. These peaks are consistently reduced within the fault zone compared to
244 the host sand. All samples show a 10Å mica (muscovite), though this is less pronounced in
245 samples from the fault zone. Samples 0401, 0402, 0407 and 0409 contain some <2µm quartz
246 (identified from the 20.92 second order peak), but it is likely that all samples contain some
247 amount of <2µm quartz. Minor peaks suggest the presence of halite and hydroxysodalite. No
248 significant peak shifts were seen in glycolated <2µm slides indicating that expandable
249 minerals are absent or insignificant in these samples.

250

251 **On the seismic character of the Riedseltz-Landau fault: A discussion**

252 The Riedseltz-Landau fault zone appears as a major tectonic structure of the western flank of
253 the northern Upper Rhine Graben. The total fault length from Soultz in France to Worms in
254 Germany reaches ~85 km and it may be subdivided in three segments: 1) the Riedseltz
255 segment from Soultz to Landau (~35 km) and along the Vosges Mountain front with a 25-km-
256 long parallel eastern Landau fault branch to the east, 2) the Lambrecht segment from Landau
257 to Leistadt that stretches for ~34 km through the pre-Permian basement rock, and 3) the
258 Worms segment from Leistadt to Wachenheim extending 16 km across the Quaternary
259 alluvial fan deposits. Although of moderate magnitude ($M_w < 5.5$), the western edge of the
260 northern URG has been the site of recurrent earthquake activity such as the 1952 earthquake
261 sequence (24/02 Io VI, 29/09 Io VI and 08/10/ Io VII, Fig. 1). In addition to our field
262 observations from the Riedseltz quarry, surface fault slip affecting late Pleistocene and
263 Holocene deposits along the fault zone by Illies and Greiner (1979), Monninger (1985) and
264 Peters (2007) support the seismogenic nature of the Riedseltz-Landau fault zone.

265 The cataclastic structures in the fault zone suggest more than one episode of
266 deformation, based on cross cutting relationships between fault rocks with different matrix
267 compositions. The earliest event (or events) was an episode of shearing that crushed grains,
268 resulting in an increase in angularity of the grains in the fault zone. Coeval or subsequent
269 dilation permitted the introduction of the prominent Fe-oxide matrix into the deformation
270 bands. A possible explanation for the lack of fine grains and the spacing between the existing
271 grains is that while the matrix was infilling the space created by the dilation, it flushed out the
272 fine grains, leaving behind only the larger grains. A subsequent fracture event produced more
273 fine grains and allowed clay matrix introduction into the deformation bands (Fig. 7 d). In this
274 most recent phase of deformation the fine grains were not flushed out, this may be due to a

275 lack of dilation or due to different hydrological conditions and the fault acting as a barrier to
276 lateral flow. Faults in unconsolidated sediments in the lower Rhine Embayment have been
277 shown to exhibit similar behaviour (Bense and Van Balen 2004). Bense et al. (2003) suggest
278 that Fe-oxide enrichment in faulted sand can be caused by repeated wetting and drying during
279 fluctuations in water table. They observe that oxides are preferentially precipitated along fine-
280 grained laminae, which will have a higher capacity to retain water by capillary action.
281 Incidentally, Behrmann et al. (2003) suggest that ongoing seismic slip along faults in the
282 Rhine Graben may have reduced the efficacy of oil and gas seals by brecciation and fracturing
283 of previously good fault seals, thereby reducing the overall hydrocarbon potential of the area.

284 Cashman and Cashman (2000), Cashman et al. (2007) and Balsamo and Storti (2011)
285 have suggested that the presence of cataclasis in shallow, unconsolidated sand, where the
286 overburden pressure should be very low, is an indicator of deformation during seismic slip.
287 The Riedseltz fault has comparable structures to other reports of faulted unconsolidated
288 sediment. A similar central mixed zone surrounded by deformation bands is observed by
289 Haynekamp et al. (1999) and Rawling et al. (2001) in the Rio Grande Rift intraplate region.
290 The fault described by Rawling and Goodwin (2003), which was deformed at burial depths up
291 to 1km, contained a much more intense zone of deformation bands than the Riedseltz fault.
292 Cashman and Cashman (2000) report grain crushing in deformation bands cutting sediments
293 buried as little as 50m (equivalent to 1MPa). Conversely, the fault reported by Balsamo and
294 Storti (2011) cutting did not contain any deformation bands, however it did contain grains
295 deformed by spalling and transgranular fracturing as well as mineralogical changes consistent
296 with heating during coseismic slip (c.f. Balsamo et al. 2014).

297 In the western edge of the northern URG, the maximum thickness of overburden at the
298 time of faulting is unknown and it is possible that the sand could have been eroded prior to
299 deposition of the loess. The potential maximum thickness of Quaternary sediments (225 m at
300 the depocentre east of Worms) drawn from the isopach map (Haimberger et al., 2005),
301 suggests that the Quaternary sediments thin towards the southwest to less than 20m close to
302 Riedseltz. Therefore the maximum likely overburden for these sands is of the order of a few
303 tens of metres. This is at least as shallow as previously reported cataclastic faults in
304 unconsolidated sands. If the hypothesis of Cashman and Cashman (2007) stands then it is
305 probable that the deformation bands and slickenlines from the exposed fault at the Riedseltz
306 quarry may record one or more seismic slip events.

307 Critical state soil mechanics can be used to constrain the overburden required for
308 localised failure, cataclasis and porosity reduction (Schultz and Siddharthan, 2005). A failure

309 envelope defined by the mean grain size and porosity of the host sediments constrains
310 whether dilation or compression is the dominant means of deformation. Critical state soil
311 mechanics combines a failure envelope with a critical state line which makes it possible to
312 constrain whether dilation or compression is the dominant means of deformation. The mean
313 grain size determined by sieving was 0.2 ± 0.1 mm and the modal grain size of the host sand is
314 125-250 μm . As no intact host sediment samples were collected, we base the porosity
315 estimates on that for unconsolidated, poorly sorted sands (25% to 35%). The porosity
316 represented by the Fe-oxide matrix is very high (>40%), whereas the areas that appear
317 crushed have very little obvious porosity (<10%).

318 Cuss et al. (2003) experimentally determined a yield envelope for Penrith sandstone
319 (grain size 129 ± 30 μm and porosity of 28%) that is appropriate to model the stresses
320 required to produce the observed structures at Riedseltz. Using the Penrith sandstone yield
321 envelope, producing the earlier dilation phase of deformation would require a change in the
322 effective mean stress and the differential stress as a result of either a decrease in pore fluid
323 pressure or an increase in overburden. The conditions to produce the later formed deformation
324 bands would require an effective mean stress of >75 MPa and a differential stress of <80
325 MPa. However, if the maximum likely overburden at the site is 20m, the maximum confining
326 pressure would only have been 0.4 MPa. An overburden equivalent to 3km is required to
327 produce the 75 MPa effective mean stress to develop the deformation bands present in the
328 Riedseltz samples. As these conditions are highly unlikely, a more plausible means would be
329 to produce the localised zones of cataclasis during seismic movement, i.e. by dynamic stress
330 changes rather than quasi-static loading through burial.

331 Distinguishing between structures that were produced by seismic slip and/or by
332 aseismic creep has critical implications for the seismic hazard analysis. This is even more
333 difficult when dealing with fault scarps in intraplate tectonic domains with high vegetation
334 cover as in the Rhine graben, and where fault slip rates do not exceed 0.3 mm/yr (Camelbeeck
335 and Meghraoui, 1998; Camelbeeck et al., 2007). The 1952 earthquake sequence of the
336 western flank of the northern URG occurred immediately west of Wissembourg - Worms fault
337 scarp Riedseltz (Fig. 1, Illies, 1981; Helm, 1995; Leydecker, 2009) suggesting that Riedseltz
338 normal fault may be associated with a seismically active fault at depth. Here, we speculate on
339 the likelihood of seismic slip along the Riedseltz fault and the magnitude of any earthquakes
340 that may have happened on it.

341 The Riedseltz normal fault is oriented NNE and it is under extension according to the
342 NE-SW extensional stress field from focal mechanisms (Plenefisch and Bonjer 1997) and

343 field observations (Bano et al., 2002; Kervyn et al., 2002). If the total vertical offset of 1.5m
344 was the maximum slip in a single event it would represent an earthquake of magnitude up to
345 Mw 6.8 (see figure 9 in Leonard, 2010). Another scenario is that the 1.5 m fault slip is
346 cumulative and represents more than one earthquake and may even include postseismic
347 movement or creep. Taking into account the observed youngest, normal fault scarp heights
348 (average 0.6 m and about half of the slip observed by Bano et al., 2002 in geophysical
349 profiles) in Riedseltz and along the Landau – Worm fault section, the 70-80 east dipping ~25-
350 km-long fault (red arrows in Fig. 2b, fault dip also visible in seismic profile of Fig. 3c) and
351 15-km-thick seismogenic layer, a simple dislocation model (Okada, 1985) suggests a
352 minimum seismic moment of $9.2 \cdot 10^{18}$ N.m, equivalent to Mw 6.6 (Fig. 8). As observed in the
353 Riedseltz quarry (this study), on geophysical profiles by Bano et al. (2002), in the
354 Klingenmünster and Barbelroth quarries (Monninger, 1985), and inferred from the geological
355 map (Fig. 3d; BRGM, 1977), the fault affects Würm loess overlaid by Holocene alluvial
356 sandy-gravel (younger than *ca* 24 ka before present according to the geological map; BRGM,
357 1977). The 1.5 m – 3.25 m vertical slip must be younger than 24 ka, giving a minimum time-
358 averaged slip rate of 0.15 – 0.32 mm/yr. These slip rates compare well to those for other faults
359 in the Rhine Graben system (Camelbeeck et al., 2007). Ferry et al., (2005) and Nivière et al.
360 (2008) examined river terraces in the southern URG and concluded that vertical fault slip
361 rates varied from 0.1 to 0.3 mm/yr. Although these slip rates fall within the values for
362 seismically active faults, it is not necessary that this slip occurred all in one event. Although
363 fault structures, deformation bands and scarp morphology all suggest one or more events with
364 coseismic slip with a minimum 5000 years recurrence interval (estimated from 0.6 m average
365 coseismic slip) for earthquakes with $M_w \geq 6.6$, aseismic slip with creep movement cannot be
366 ruled out.

367

368 **Conclusions**

369 The Riedseltz-Landau fault is identified as a major active segment of the western flank
370 of the northern Upper Rhine Graben. The Riedseltz fault segment 25-km-long and appears as
371 a linear strand at the frontal topography of the Vosges Mountains showing prominent
372 triangular facets and affecting late Quaternary alluvial and fluvial deposits. The fault affects
373 late Pleistocene and Holocene alluvial units (Illies and Greiner, 1979; Monninger, 1985;
374 Weidenfeller and Zöller, 1995; Peters, 2007) and shows about 1.5 m slip in shallow
375 geophysical profiles (Bano et al., 2002). Field investigations on fault scarp morphology

376 combined with the study of the fault exposure in the Riedseltz quarry indicate repeated
377 cataclastic slip and fracturing on a narrow zone of deformation.

378 Detailed microstructure and mineralogical studies of the fault cataclasite using the
379 analysis of SEM and XRD images indicate deformation bands in mixed zones with low grain
380 size and slip surfaces with grain size reduction and streaked out bands due to oxide
381 concentration. The deformation bands also appear with highly fractured grains showing
382 spalling and transgranular fractures in quartz that illustrate the intense shearing and the
383 possible seismic slip in the fault zone. The fault structures and related cataclasis suggest two
384 phases of deformation with 1) shearing, grain crushing and porosity reduction within
385 deformation bands 2) emplacement of the prominent Fe-oxide matrix into the fault zone,
386 possibly accomplished by flushing out of fine grains, and 3) at least one further fracturing
387 episode producing more fine grains and allowing clay matrix emplacement. The presence of
388 cataclastic deformation bands shows that that localized failure occurred despite the minimal
389 overburden (< 20m). Cataclasis could be a very helpful indicator for seismic slip in shallowly
390 buried sediments but more work is required to further constrain the micromechanics of
391 cataclasis under very low confining stress.

392 The fault scarp and surface deformation bands may be related to successive seismic
393 slip but we cannot rule out the existence of aseismic slip. Further paleoseismic investigations
394 are required to determine the relative amounts of seismic and aseismic slip along the
395 Riedseltz-Landau fault segment. For the moment, a simple fault model suggests a minimum
396 Mw 6.6 earthquake as a plausible scenario for seismic slip along the western edge of the
397 northern Upper Rhine Graben.

398

399

400

401

402

403 **Acknowledgements**

404 We thank Kenny Roberts, Peter Chung John Gilleece and Caroline Smith for their technical
405 expertise; Matthieu Ferry, Tony Nemer, Pierre-Jean Alasset and Justin Erickson for field
406 assistance; Martin Lee and Colin Braithwaite for assistance with sedimentary structures. XRD
407 samples were prepared and run by Robbie Goodhue of Trinity College, Dublin. We thank
408 Kurt Decker and Ramon Arrowsmith for their review of manuscript. Collaboration between
409 ZKS and MM was facilitated by the EOST-IPGS (CNRS-UMR 7516) visitor programme and
410 the Ulysses Ireland-France EGIDE-CAMPUS research visit scheme.

411

412 **References**

- 413 Baize, S., Cushing, M., Lemeille, F., Jomard, E. 2013. Updated seismotectonic zoning scheme
414 of Metropolitan France, with reference to geologic and seismotectonic data. *Bull. Soc.
415 geol. Fr.*, 184, n°3, 225-259.
- 416 Balsamo F. and Storti, F. 2011. Size-dependent comminution, tectonic mixing and sealing
417 behaviour of a “structurally oversimplified” fault zone in poorly lithified sands: Evidence
418 for a coseismic rupture? *Geological Society of America Bulletin*, 123, p. 601-619. doi:
419 10.1130/B30099.1
- 420 Balsamo, F., Aldega, L., De Paola, N., Faoro, I. & Storti, F. (2014). The signature and
421 mechanics of earthquake ruptures along shallow creeping faults in poorly lithified
422 sediments. *Geology* 42, 435-438. doi: [10.1130/G35272.1](https://doi.org/10.1130/G35272.1)
- 423 Bano M., Edel J.-B., Herquel G. and EPGs Class 2001-2002. 2002. Geophysical investigation
424 of a recent shallow fault. *The Leading Edge*, 21, 648-650. doi: 10.1190/1.1497317
- 425 Behrmann J. H., Hermann O., Horstmann M., Tanner D.C., and Bertrand G. 2003. Anatomy
426 and kinematics of oblique continental rifting revealed: A three-dimensional case study of
427 the southeast Upper Rhine graben (Germany). *AAPG Bulletin*, 87, 1105–1121.
- 428 Bense V. F. and Van Balen, R. T. 2004. The effect of fault relay and clay smearing on
429 groundwater flow patterns in the Lower Rhine Embayment. *Basin Research*, 16, 397–411.
- 430 Bense, V.F., Van den Berg, E.H., Van Balen, R.T. 2003. Deformation mechanisms and
431 hydraulic properties of fault zones in unconsolidated sediments; the Roer Valley Rift
432 System. *The Netherlands Hydrogeology Journal*, 11, 319-332.
- 433 Bonjer, K.-P., Gelbke, C., Gilg, B., Roulard, D., Mayer-Rosa, D., Massinon, B. 1984.
434 Seismicity and dynamics of the Upper Rhine graben. *Journal of Geophysics* 55, 1–12.
- 435 BRGM, 1977, Carte Géologique Seltz-Wissembourg (1/50 000), N°199, Bureau de Recherche
436 Géologique et Minière, 75015 Paris, France.
- 437 Brun, J. P., Gutscher M. A. and DEKORP-ECORS teams. 1992. Deep crustal structure of the
438 Rhine Graben from DEKORP-ECORS seismic reflection data: a summary.
439 *Tectonophysics*, 208, 139-147.
- 440 Camelbeeck T, and Van Eck T. 1994. The Roer Valley Graben earthquake of 13 April 1992
441 and its seismotectonic setting, *Terra Nova*, 6, 291-300.
- 442 Camelbeeck T, Meghraoui M. 1998. Geological and geophysical evidence for large
443 paleoearthquakes with surface faulting in the Roer Graben (northwest Europe). *Geophys.
444 J. Int.*, 132, 347-362.
- 445 Camelbeeck, T., Vanneste, K. et al. 2007. Relevance of active faulting and seismicity studies
446 to assess longterm earthquake activity in Northwest Europe. In: Stein, S.&Mazzotti, S.
447 (eds) *Continental Intraplate Earthquakes: Science, Hazard, and Policy Issues*. Geological
448 Society of America, Special Papers, 425, 193–224.
- 449 Cara, M., Cansi, Y., Schlupp, A. et al. 2015. SI-Hex: a new catalogue of instrumental
450 seismicity for metropolitan France. *Bull. Soc. géol. France*, t. 186, no 1, 3-19,
451 doi:10.2113/gssgfbull.186.1.3.

- 452 Cashman, S., Cashman, K. 2000. Cataclasis and deformation formation in unconsolidated
453 marine terrace sand, Humboldt County, California. *Geology*, v. 28, no. 2, 111-114.
- 454 Cashman S.M., Baldwin J. N., Cashman K.V., Swanson K. and Crawford R. 2007.
455 Microstructures developed by coseismic and aseismic faulting in near-surface sediments,
456 San Andreas fault, California. *Geology*, 35, 611–614; doi: 10.1130/G23545A.1
- 457 DoebI, F. 1970. Die tertiären und quartären Sedimente des südlichen Rheingrabens. In: Illies,
458 J.H., Mueller, S. (Eds.), Graben Problems. Proceedings of an International Rift
459 Symposium held in Karlsruhe October, 10–12, 1968. E. Schweizerbart'sche, Stuttgart,
460 56–66.
- 461 Evans, J. P., & Bradbury, K. K. 2007. Fractured dirt: Deformation textures and processes in
462 sediment and other unconsolidated deposits. *Geology*, 35(7), 671-672.
- 463 Farr, T.G., Kobrick, M. 2000. Shuttle Radar Topography Mission produces a wealth of data.
464 *Eos. Trans. AGU*, 81, 583–585.
- 465 Ferry M., Meghraoui M., Delouis B. and Giardini D. 2005, Evidence for Holocene
466 Paleoseismicity along the Basel-Reinach Active Normal Fault (Switzerland): A Seismic
467 Source for the 1356 Earthquake in the Upper Rhine Graben. *Geophys. J. Int.*, 158, 1-21.
- 468 Fossen H., Schultz R. A., Shipton Z. K. and Mair K. 2007. Deformation bands in sandstone –
469 a review. *Journal of the Geological Society*, 164, 755–769.
- 470 Fuhrmann, T., Heck, B., Knöpfler, A., Masson, F., Mayer, M., Ulrich, P. Westerhaus, M.,
471 Zippelt, K. 2013. Recent surface displacements in the Upper Rhine Graben - Preliminary
472 results from geodetic networks. *Tectonophysics*, 602(0), 300–315.
- 473 Grützner, C., Fischer, P. and Reicherter, K., 2016. Holocene surface ruptures of the Rurrand
474 Fault, Germany—insights from palaeoseismology, remote sensing and shallow
475 geophysics. *Geophys. J. Int.* (2016) 204, 1662–1677, doi: 10.1093/gji/ggv558
- 476 Haimberger, R., Hoppe, A., Schäfer, A. 2005. High-resolution seismic survey on the Rhine
477 River in the northern Upper Rhine Graben. *Int. J. Earth Sci.* 94, 657–668.
- 478 Helm J. A. 1995. The Natural Seismic Hazard and Induced Seismicity of the European Hot
479 Dry Rock Geothermal Energy Project at Soultz-sous-Fôrets (Bas-Rhin, France),
480 Unpublished PhD thesis, Ecole et Observatoire de Physique du Globe de Strasbourg,
481 France. 197 pp.
- 482 Heynekamp, M.R., Goodwin, L.B., Mozley, P.S., Haneberg, W.C. 1999. Controls on fault-
483 zone architecture in poorly lithified sediments, Rio Grande Rift, New Mexico:
484 implications for fault-zone permeability and fluid flow. In: Haneberg, W.C., Mozley, P.S.,
485 Moore, J.C., Goodwin, L.B. (Eds.), *Faults and Subsurface Fluid Flow in the Shallow
486 Crust*. American Geophysical Union Geophysical Monograph, 113, 27-49.
- 487 Illies, J. H., and Greiner, G., 1979. Holocene movements and state of stress in the
488 Rhinegraben rift system. *Tectonophysics* 52, 349-359.
- 489 Illies J. H. 1981. Mechanism of graben formation. *Tectonophysics*, 73, 249-266.
- 490 Kervyn, F., M. Ferry, P. J. Alasset, E. Jacques, and M. Meghraoui. 2002. The potential for
491 large earthquakes in intraplate Europe: the contribution of remote sensing, EGS Meeting
492 With Abstract (Poster), Nice, France.
- 493 Lemeille F., Cushing M. E., Cotton F., et al. 1999. Evidence for Middle to Late Pleistocene
494 faulting within the northern Upper Rhine Graben (Alsace Plain, France). *Earth and
495 Planetary Science*, 328, 839-846.

- 496 Leonard, M. 2010. Earthquake Fault Scaling: Self-Consistent Relating of Rupture Length,
497 Width, Average Displacement, and Moment Release, *Bull. Seism. Soc. America* 100, No.
498 5A, pp. 1971–1988, doi: 10.1785/0120090189.
- 499 Leydecker, G. 2009. Earthquake Catalogue for the Federal Republic of Germany and Adjacent
500 Areas for the Years 800–2002—Datafile, <http://www.bgr.de/quakecat> — Federal Institute
501 for Geosciences and Natural Resources. Hannover, Germany.
- 502 Masson, F., Knoepfler, A., Mayer, M., Ulrich, P., Heck, B. 2010, Upper bounds of
503 deformation in the Upper Rhine Graben from GPS data - First results from GURN
504 (GNSS Upper Rhine Graben Network), EGU General Assembly 2010, held 2-7 May,
505 2010 in Vienna, Austria, p.4516.
- 506 Meghraoui M., Delouis B., Ferry M., et al. 2001. Active normal faulting in the upper Rhine
507 graben and paleoseismic identification of the 1356 Basel earthquake. *Science*, 293, 2070-
508 2073.
- 509 Meghraoui M., Camelbeeck T., Vanneste K., et al. 2000. Active faulting and paleoseismology
510 along the Bree fault, lower Rhine graben, Belgium. *J. Geophys. Res.*, 105, 13809-13841.
- 511 Monninger, R., 1985, Neotektonische bewegungsmechanismen in mittleren Oberrheingraben,
512 PhD Thesis dissertation, Fakultät von Bio- und Geowissenschaften, pp. 219.
- 513 Nivière et al. 2008. Active tectonics of the southeastern Upper Rhine Graben, Freiburg area
514 (Germany). *Quaternary Science Review*, 27, 541-555.
- 515 Okada, Y. 1985. Surface deformation due to shear and tensile faults in a half-space. *Bull.*
516 *Seismol. Soc. Am.*, 75, 1135–1154.
- 517 Petrik, A., Beke, B., & Fodor L. 2014. Combined analysis of faults and deformation bands
518 reveals the Cenozoic structural evolution of the southern Bükk foreland (Hungary).
519 *Tectonophysics*, 633, 43–62.
- 520 Peters G., Buchmann T.J., Connolly P., van Balen R. T., Wenzel F., Cloetingh S. 2005.
521 Interplay between tectonic, fluvial and erosional processes along the Western Border Fault
522 of the northern Upper Rhine Graben, Germany. *Tectonophysics*, 406, 39-66.
- 523 Peters, G., 2007, Active tectonics in the upper Rhine graben, PhD dissertation, Free
524 University of Amsterdam, pp. 270.
- 525 Plenefisch, T. and K.-P. Bonjer. 1997. The stress field of the Rhine Graben area inferred from
526 earthquake focal mechanisms and estimation of frictional parameters. *Tectonophysics*,
527 275, 71-97.
- 528 Rawling, G.C., Goodwin, L.B. 2003. Cataclasis and particulate flow in faulted, poorly
529 lithified sediments. *Journal of Structural Geology*, 25, 317-331.
- 530 Rawling, G.C., Goodwin, L.B. 2006. Structural record of the mechanical evolution of mixed
531 poorly lithified sediments, Rio Grande rift, New Mexico. *Journal of Structural Geology*,
532 28, 1623-1639.
- 533 Rawling, G.C., Goodwin, L.B., Wilson, J.L., 2001. Internal architecture, permeability
534 structure, and hydrologic significance of contrasting fault-zone types. *Geology* 29, 43-46.
- 535 Sallet E. and Wibberley C.A.J. 2010. Evolution of cataclastic faulting in high-porosity
536 sandstone, *Bassin du Sud-Est*, Provence, France. *Journal of Structural Geology*, 32,
537 1590–1608 doi:10.1016/j.jsg.2010.02.007

- 538 Schultz, R.A., and Siddharthan, R., 2005, A general framework for the occurrence and
539 faulting of deformation bands in porous granular rocks: *Tectonophysics*, v. 411, p. 1–18,
540 doi: 10.1016/j.tecto.2005.07.008.
- 541 Sigda, J.M., Goodwin, L.B., Mozley, P.S., Wilson, J.L. 1999. Permeability alteration in small-
542 displacement faults in poorly lithified sediments: Rio Grande Rift, Central New Mexico.
543 In: Haneberg, W.C., Mozley, P.S., Moore, J.C., Goodwin, L.B. (Eds.), *Faults and*
544 *Subsurface Fluid Flow in the Shallow Crust*. American Geophysical Union Geophysical
545 *Monograph*, 113, 51-68.
- 546 Sisfrance, Seismicity catalogue of France, <http://www.sisfrance.net>, last accessed 18 June
547 2015.
- 548 Stein, S., Liu, M., Camelbeeck, T., Merino, M., Landgraf, A., Hintersberger, E., & Kuebler,
549 S., 2015, Challenges in assessing seismic hazard in intraplate Europe: in Landgraf, A.,
550 Kuebler, S., Hintersberger, E. & Stein, S. (eds), *Seismicity, Fault Rupture and Earthquake*
551 *Hazards in Slowly Deforming Regions*. Geological Society, London, Special
552 *Publications*, 432, doi :org/10.1144/SP432.7
- 553 Vanneste, K., Verbeeck, K., Camelbeeck, T., Renardy, F., Meghraoui, M., Jongmans, D.,
554 Paulissen, E., and Frechen, M., 2001, Surface rupturing history of the Bree fault
555 escarpment, Roer valley graben: New trench evidence for at least six successive events
556 during the last 150 to 185 kyr: *Journal of Seismology*, v. 5, p. 329–359, doi:
557 10.1023/A:1011419408419.
- 558 Weidenfeller, M. and Zöller, L., 1995. Mittelpleistozäne tektonik in einer Lös-Paläoboden-
559 Abfolge am westlichen Rand des Oberrheingraben. *Mainzer geowiss.Mitt.* 24, 87-102.

560
561
562
563
564

565 **Figure Captions**

566

567 Fig. 1. The Upper Rhine Graben instrumental and historical seismicity: blue circles are
568 seismicity from 1960 to 2012 and yellow boxes are seismicity from AD 800 to 1960
569 (Leydecker, 2009 and SiHex catalogue, Cara et al., 2015). Note the location of the 1952
570 earthquake sequence (light brown; Leydecker, 2009). The box outlines the location of Fig. 2a.
571 The topography is an extract of the SRTM 3-arc-second (~90 m) posting digital elevation
572 model (Farr and Kobrick, 2000). The inset shows the study area in continental Europe.

573

574 Fig. 2. a) Tectonic morphology using SRTM digital topography (see Fig. 1 for location) along
575 the western URG and location of the Riedseltz fault (black arrows). The Riedseltz fault joins
576 the Worms fault scarp (WFS) to the north. This fault zone crosses the Riedseltz quarry (box is
577 for geological map of Fig. 2d) and extends to the north towards Worms and Wacheheim. The
578 red arrows mark the location of a possible parallel fault branch and related scarp. The dashed
579 line is location of seismic profile of figures 2 b and c.

580 b) Seismic profile (commercial) and c) interpreted seismic profile with illustrated fault offsets
581 at depth. Located immediately east of Wissembourg, the profile displays normal faults that
582 seem to reach the surface and affect Oligocene-Miocene units at depth (green and orange
583 layers). Note the slight vertical exaggeration so the fault dips are about 70° to 80°.

584 d) Geological map of the southern extension of Riedseltz fault and quarry area. 1: Sandstone
585 and clay of the Trias Substratum of the Vosges mountains; 2: Clay units of Oligocene, 3:

586 Pliocene sandy clay and gravel deposits, 4: Late Quaternary alluvial sand, gravel and loess
587 (Riss and Würm), 5: Holocene colluvial and alluvial deposits, 6: Peat of marsh areas with
588 sandy-silt alluvial units, 7: Neogene and Quaternary fault, 8: Late Quaternary and Holocene
589 fault scarp (seismogenic fault zone).

590
591 Fig. 3. a) Panorama of the Riedseltz quarry showing nature of quarry host units and position
592 of fault (white arrows). Seated figure to the right of the fault for scale.
593 b) Interpretive sketch of fault zone next to c) field photograph. The grey lines in b) indicate
594 the geometry of the cataclastic deformation bands. The black crosses are markers at 1 m grid
595 spacing on the outcrop – note that the grid in c) is distorted due to the 3D nature of the
596 outcrop face. Inset stereonet (lower hemisphere) shows the geometry of fault and bedding
597 planes.

598
599 Fig. 4. Details of hand specimens. a) Deformation bands are the paler bands about 1mm wide
600 running vertically in this image. They split about half way up this sample with an
601 anastomosing geometry common in deformation bands (Fossen et al 200). They are
602 marginally more consolidated than the sediment around them and stand slightly proud of the
603 surface.
604 b) View onto a slip surface face showing streaked out oxides along the slip surfaces. The
605 streaks are oriented vertically in this figure.

606
607 Fig. 5. Deformation bands with reduced grain size. a) whole thin section showing deformation
608 bands running right to left. Note the mottled colour staining at the bottom of the thin section.
609 Arrow shows location for sampling in b and c. Scale bar = 1cm. b) Plain polarised light (scale
610 bar 1 mm across), and c) backscatter electron SEM image of deformation band from this
611 section, showing intense grain size reduction along the margin.

612
613 Fig 6. SEM backscatter images of spalling (sp) at grain margins and transgranular fractures
614 (tg). Note the later coating of clay around the grains, which post-dates the spalling.

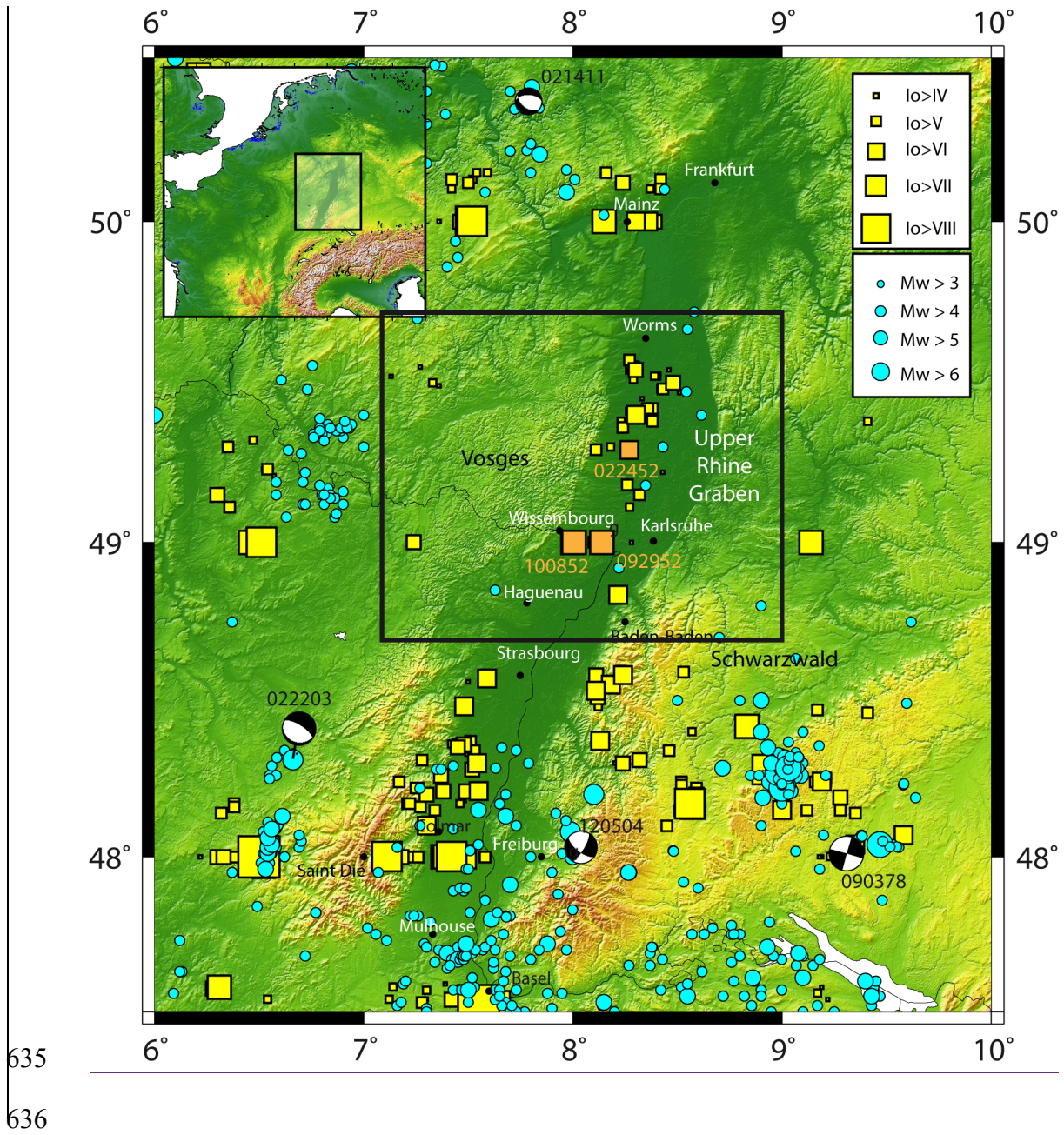
615
616 Fig. 7. Typical colour variations of the matrix. a) Clay matrix in plain polarised light, and b)
617 Backscatter SEM, note the reduced grain size. c) Boundary between region of Fe-oxide matrix
618 and clay matrix and (d) Fe-oxide matrix with clay filled fracture (arrowed), few fine grains
619 and little/no grain contacts. Photomicroscope images are plain polarised light and the scale
620 bars are 1 mm across.

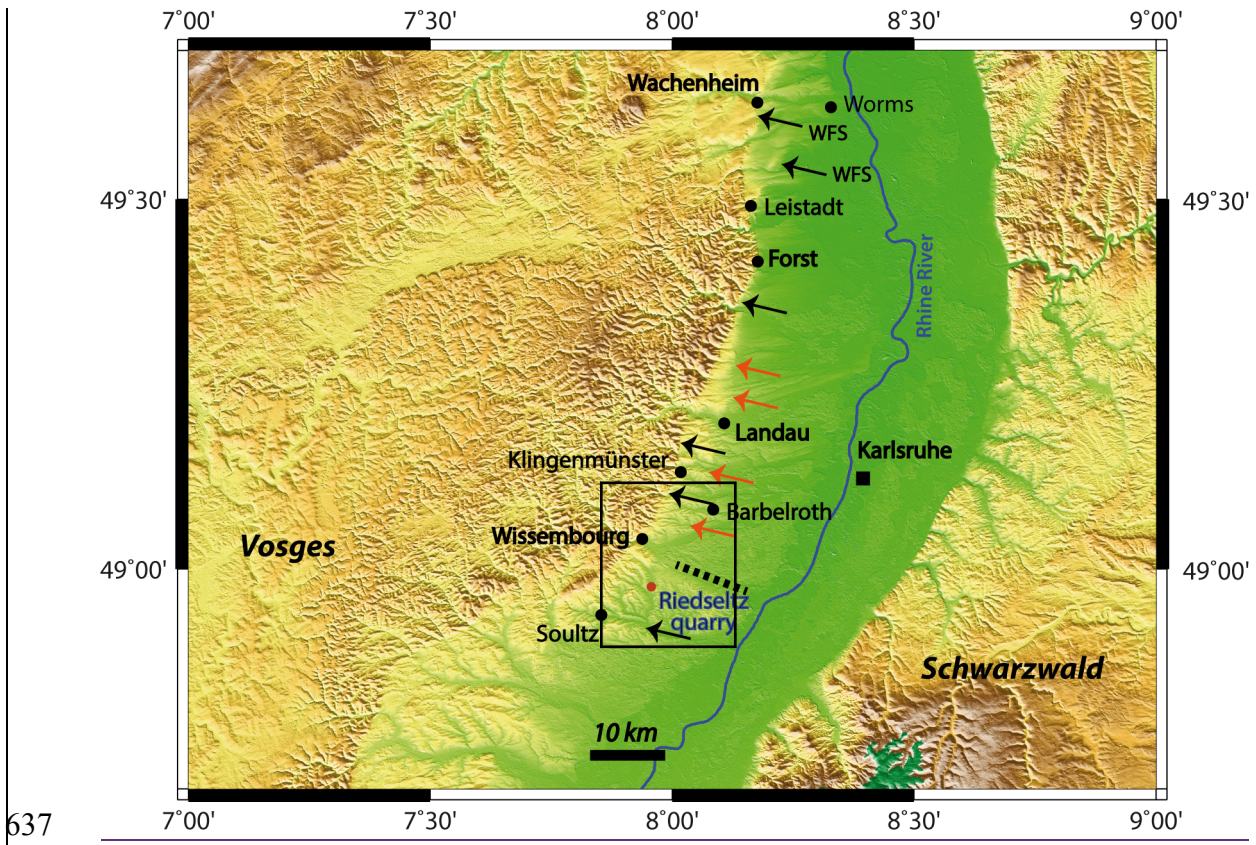
621
622 Fig. 8. XRD data for samples from the footwall (top, black traces), hangingwall (middle, grey
623 traces) and fault zone (bottom, black traces). The fault zone seems enriched in halite and to
624 have reduced kaolinite with respect to the host rocks.

625
626 Fig. 9. a) EDX element map of the deformation bands shows iron-rich cement concentrated in
627 fine grained layers (Green = Fe; Red = Ca; Blue = Al). Iron concentration is not always along
628 slip-surfaces. b) Backscatter SEM image of the same area.

629
630 Fig. 10. Dislocation model (using Okada, 1985) applied to the 25-km-long fresh scarp of the
631 Riedseltz normal fault segment (strike: 15°N, Dip: 75 east, rake: -90, average slip: 0.6 m; see
632 also Fig. 2b), suggesting an earthquake magnitude Mw 6.64. Black box is Riedseltz quarry
633 location.

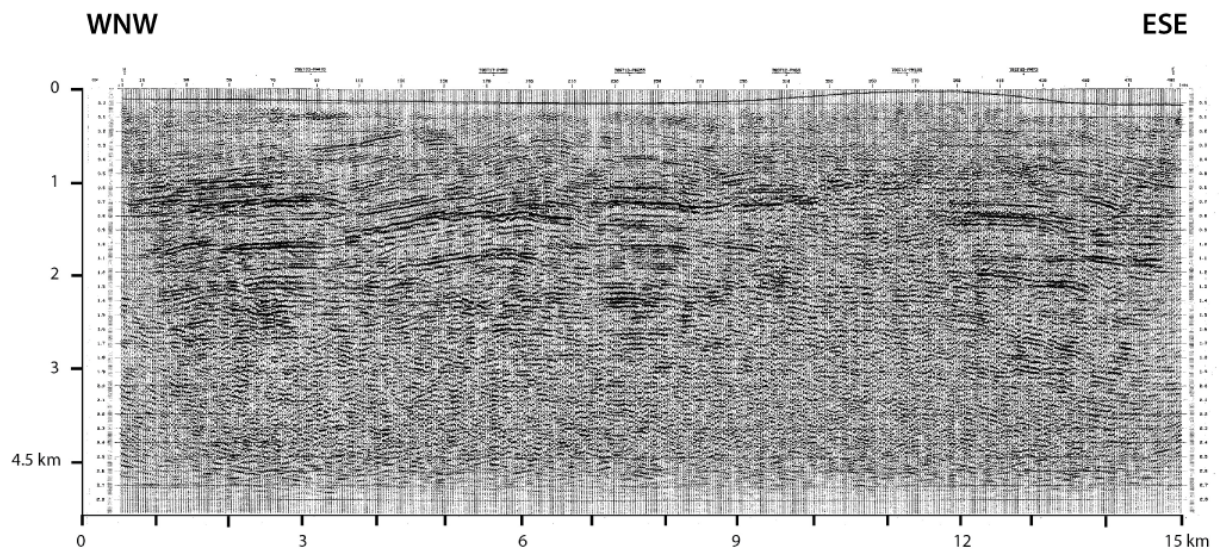
634



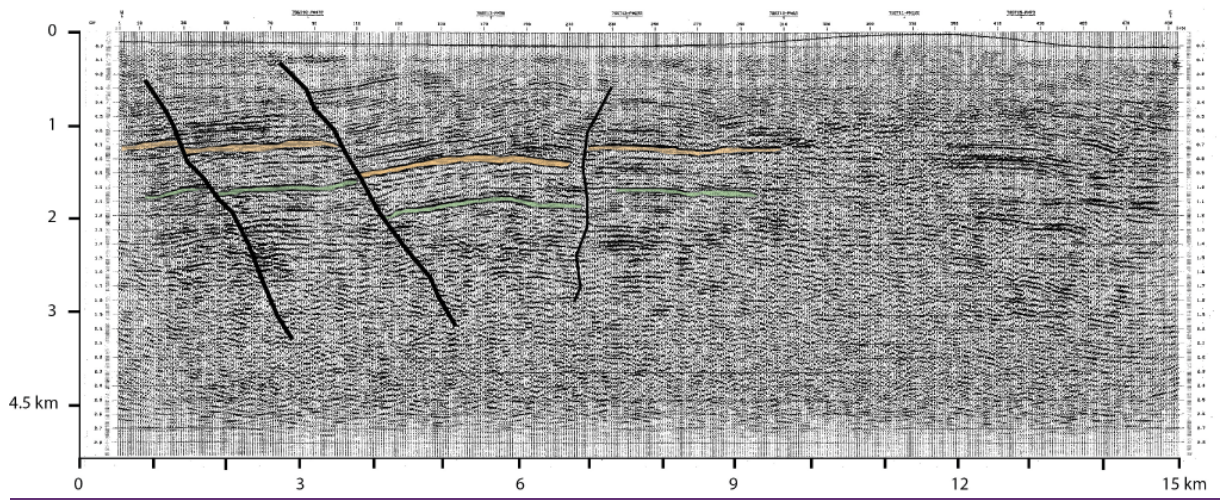


637

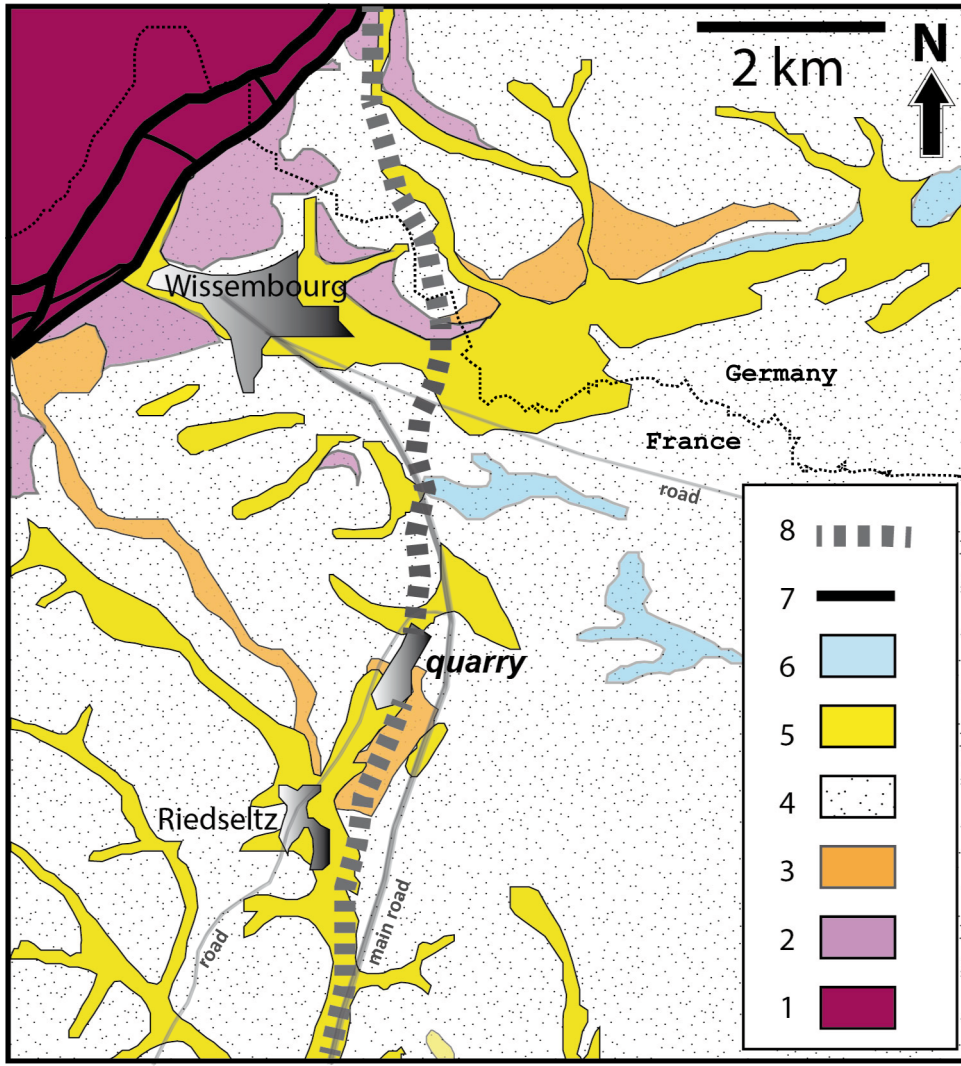
b)

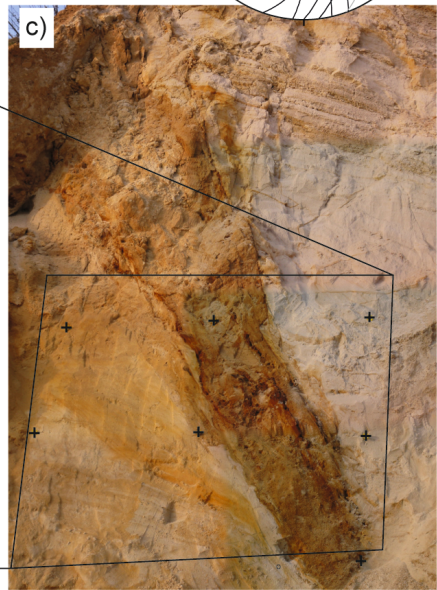
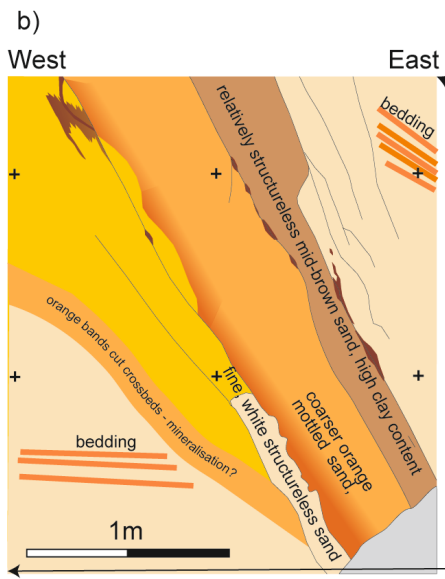
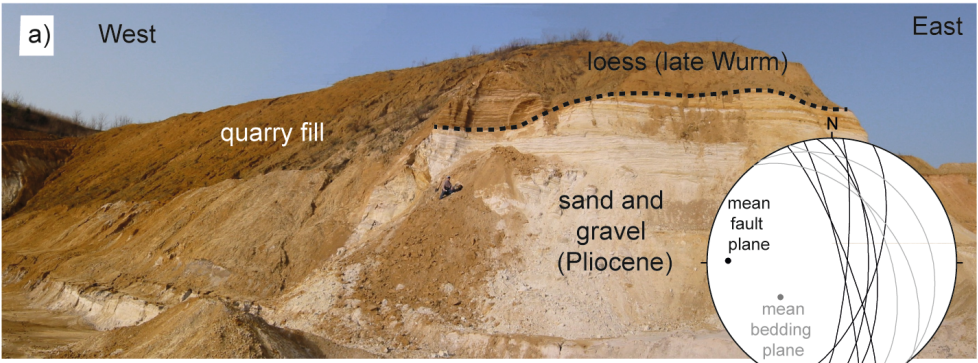


c)



638



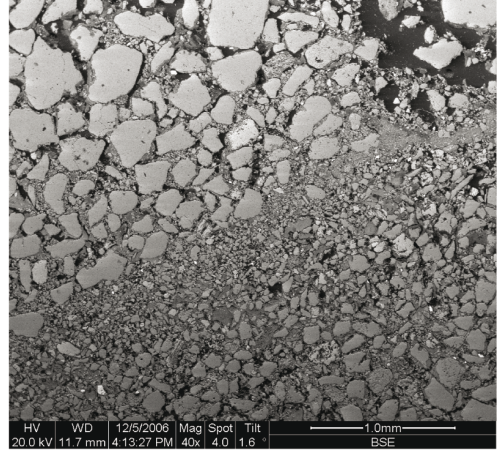
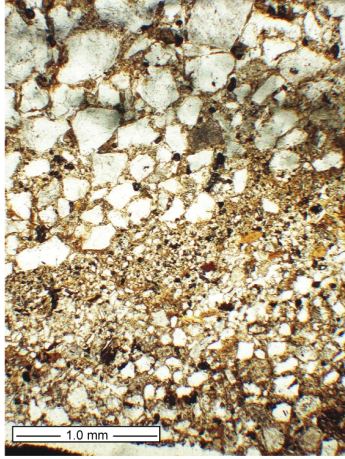
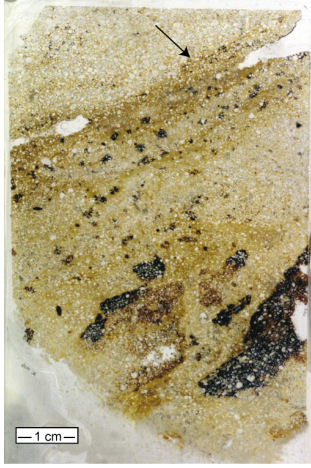


640

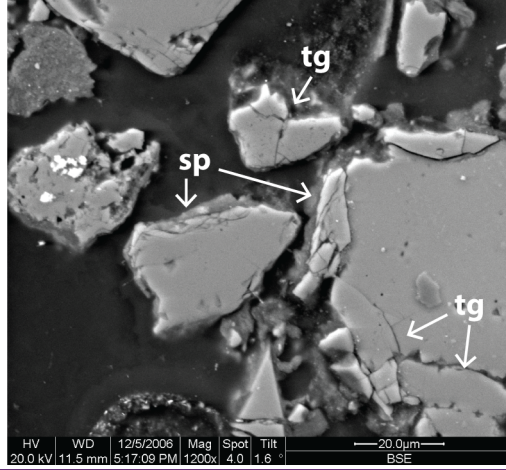
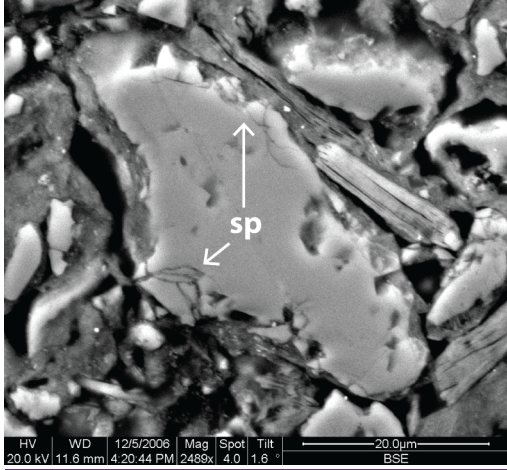


641

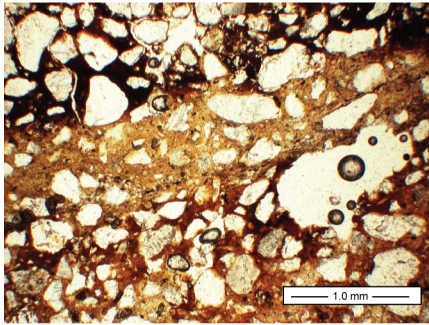
642



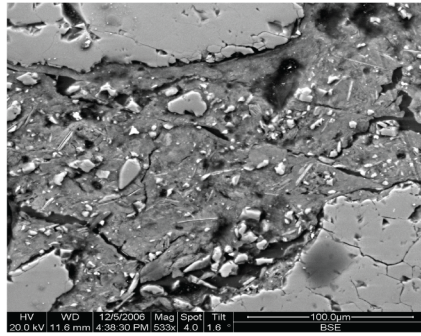
643



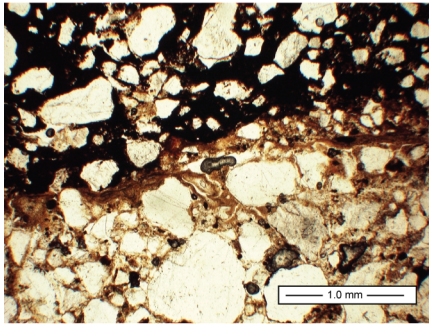
a)



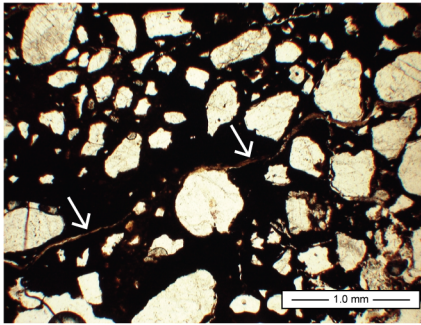
b)



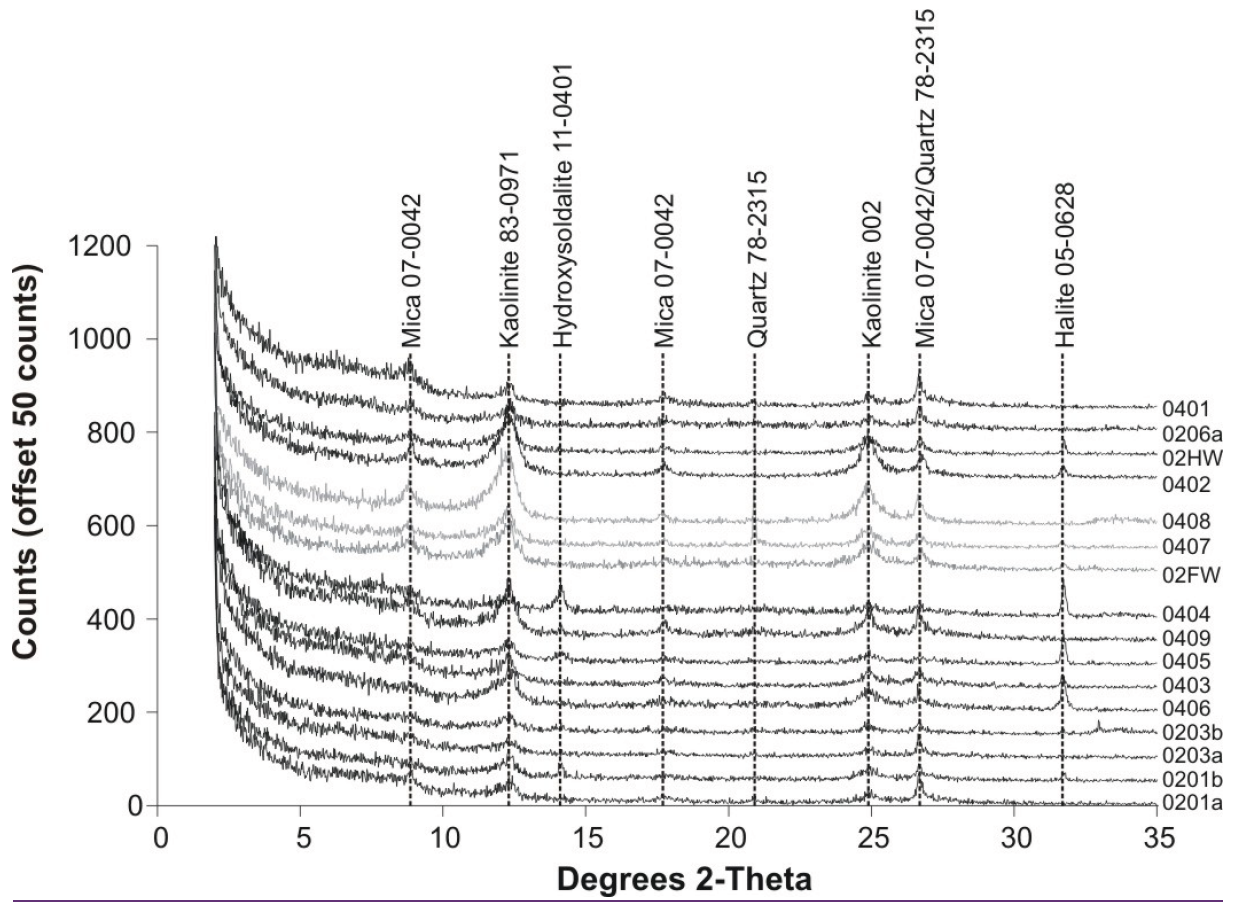
c)



d)

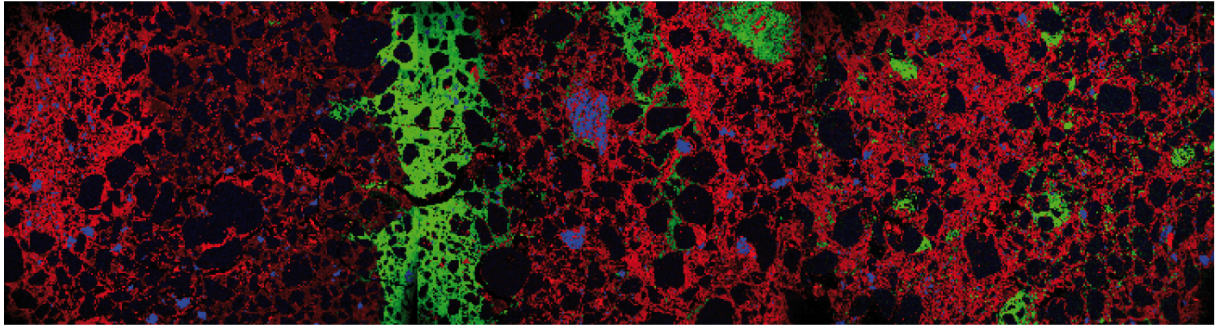


644

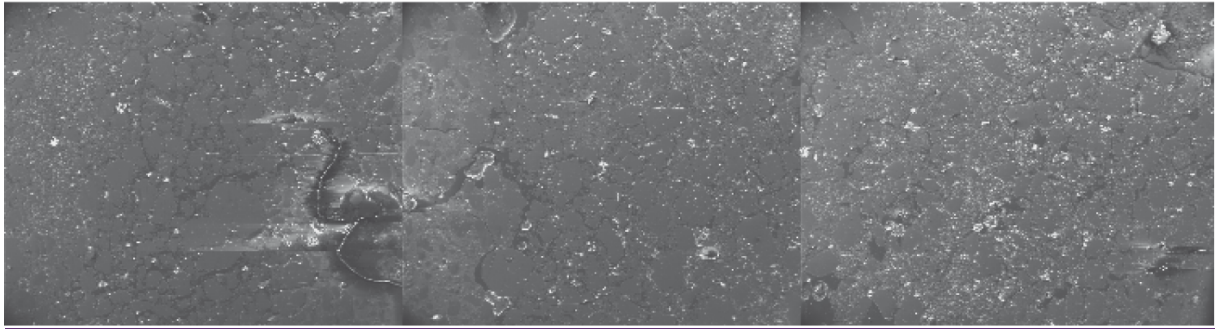


645

a)



b)



646

